RESEARCH ARTICLE

PROTEINS WILEY

Characterization of the multidrug efflux transporter styMdtM from *Salmonella enterica* serovar Typhi

Aqsa Shaheen[1,2,3] | Fouzia Ismat[1] | Mazhar Iqbal[1] | Abdul Haque[1,4] | Zaheer Ul-Haq[5] | Osman Mirza[6] | Rita De Zorzi[3,7] | Thomas Walz[3,8] | Moazur Rahman[1,3,9]

[1]Drug Discovery and Structural Biology Group, Health Biotechnology Division, National Institute for Biotechnology and Genetic Engineering (NIBGE), Faisalabad, Punjab, Pakistan

[2]Department of Biochemistry and Biotechnology, University of Gujrat, Gujrat, Punjab, Pakistan

[3]Department of Cell Biology, Harvard Medical School, Boston, Massachusetts

[4]Akhuwat First University, Faisalabad, Punjab, Pakistan

[5]Dr. Panjwani Center for Molecular Medicine and Drug Research, International Center for Chemical and Biological Sciences, University of Karachi, Karachi, Sindh, Pakistan

[6]Department of Drug Design and Pharmacology, Faculty of Health and Medical Sciences, University of Copenhagen, Copenhagen, Denmark

[7]Department of Chemical and Pharmaceutical Sciences, University of Trieste, Trieste, Italy

[8]Laboratory of Molecular Electron Microscopy, Rockefeller University, New York, New York

[9]School of Biological Sciences, University of the Punjab, Lahore, Punjab, Pakistan

Correspondence
Thomas Walz, Laboratory of Molecular Electron Microscopy, Rockefeller University, New York, NY, USA.
Email: twalz@rockefeller.edu

Moazur Rahman, School of Biological Sciences, University of the Punjab, Lahore, Punjab, Pakistan.
Email: moazur.rahman@fulbrightmail.org

Funding information
Foundation for the National Institutes of Health, Grant/Award Number: U54 GM094598; Higher Education Commission, Pakistan, Grant/Award Number: 20-1504

Abstract

Salmonellae are foodborne pathogens and the major cause of gastroenteritis in humans. *Salmonellae* express multidrug efflux transporters that play a key role in their drug resistance, which is becoming an increasing problem for therapeutic intervention. Despite their biomedical importance, the mechanisms underlying substrate transport by multidrug efflux transporters remain poorly understood. Here, we describe the first characterization of a multidrug transporter belonging to the major facilitator superfamily from the genus *Salmonella*. We show that several clinical *Salmonella* Typhi (*S.* Typhi) isolates constitutively express the *styMdtM* (*STY4874*) gene, which encodes a known multidrug-resistance (MDR) transporter. Guided by the structure of the *Escherichia coli* (*E. coli*) homolog, we studied two residues critical for substrate transport, Asp25 and Arg111. Mutation of Asp25 to glutamate did not affect the transport function of styMdtM, whereas mutation to alanine reduced its transport activity, suggesting that a negative charge at this position is critical for substrate translocation across the membrane. Substrate-affinity measurements by intrinsic fluorescence spectroscopy showed that the Asp25Ala mutant retained its capacity to bind substrate, albeit at a lower level. Mutation of Arg111 to alanine resulted in a decrease in secondary structure content of the transporter, and mutation to lysine completely destabilized the structure of the transporter. A homology model of styMdtM suggests that Arg111 is important for stabilizing the transmembrane domain by mediating necessary interactions between neighboring helices. Together, our studies provide new structural and mechanistic insights into the *Salmonella* MDR transporter styMdtM.

KEYWORDS

E. coli MdfA, efflux pump, foodborne pathogen, MdtM, multidrug resistance, *Salmonella* Typhi

1 | INTRODUCTION

Salmonellae are important foodborne pathogens that have been reported to contaminate various food products, ranging from poultry to seafood and vegetables. With over 2500 serovar, *Salmonellae*, including

Salmonella enterica serovar Typhi (*S.* Typhi) and *Salmonella enterica* serovar Paratyphi, have a long history of afflicting humans, in which they cause severe gastroenteritis and systemic infections.[1] *Salmonella* epidemics remain a serious problem in developing countries to this day,[1,2] and combatting the disease is made difficult by several gaps in our knowledge of these pathogens. One such gap lies in our understanding of multidrug-resistance (MDR) exporters in *Salmonella* sp, which constitute one of the major mechanisms for their adaptive resistance.[3]

The World Health Organization has identified the emergence of MDR in pathogenic bacteria as a major threat to public health,[4] and microbes with enhanced resistance to one or more antibiotic(s) routinely recommended for their treatment in clinical settings are now commonly known as "superbugs."[5,6] Pathogens can acquire drug resistance through different mechanisms, such as by changes in the drug target, inactivation of the drug itself, a decrease in the outer membrane permeability for the drug, and increased export of the drug out of the cell. Increased drug export, mediated by MDR transporters, lowers the drug concentration in the cytoplasm and is an important mechanism used by superbugs.[7] Many of the involved transporters have a wide substrate specificity, which enables them not only to expel a wide range of antibiotics out of the cell, but also forms the basis for the acquisition of additional resistance determinants.[4]

Salmonellae possess multiple drug-efflux systems. The AcrAB-TolC system, which belongs to the resistance nodulation division superfamily, is the major housekeeping efflux system.[8,9] This efflux system has been identified in many *Salmonella* serovars, including *Salmonella* Typhimurium, *Salmonella* Enteritidis, *Salmonella* Kentucky, *Salmonella* Heidelberg, *Salmonella* Choleraesuis, *Salmonella* Schwarzengrund, *Salmonella* Haardt, and *Salmonella* Istanbul,[10-13] and is the only efflux system that has so far been studied in *Salmonellae*. *Salmonellae* also express other MDR transporters, including members of the major facilitator superfamily (MFS), such as MdfA, EmrAB, and MdtK in *S.* Typhimurium,[14] and STY4874 in *S.* Typhi,[15] but none of these MFS transporters has so far been studied in any detail. A full understanding of the structure and function of these additional MDR transporters will be essential; however, to develop inhibitors against them, thus ensuring the efficacy of administered antibiotics.

In a previous study, we identified MFS-type MDR transporters in *S.* Typhi and found that STY4874—now referred to as styMdtM, owing to its high degree of sequence homology with *Escherichia coli* (*E. coli*) MdtM (ecMdtM)—has a particularly broad substrate spectrum.[15] We then reported that styMdtM is inhibited by phyto extracts.[16] In the present study, we aimed at understanding structural and functional aspects of this potentially important resistance determinant. In particular, we set out to elucidate the role of two residues, Asp25 and Arg111 that are of critical importance for the function of the homologous *E. coli* transporters.

2 | MATERIALS AND METHODS

2.1 | Quantitative real-time reverse transcriptase PCR

Overnight bacterial cultures were diluted 1:100 in fresh LB broth and grown at 37°C to mid-logarithmic phase ($A_{600} = 0.5$-0.6). Total RNA was extracted from *S.* Typhi isolates using One Step-RNA Reagent (Bio-Basic: BS410A) and treated with DNase I (Thermo Fischer, MA, USA). The RNA samples were quantified and 0.5 μg of DNase-treated RNA was used for cDNA synthesis using the mixture of single-stranded random 6-nucleotide primers and reverse transcriptase in cDNA Synthesis Kit (Thermo Fisher, MA, USA). Quantitative real-time reverse transcriptase PCR (qRT-PCR) was then performed to measure the expression of the *styMdtM* gene in *S.* Typhi isolates relative to that of the enolase housekeeping gene. A total volume of 25 μL reaction mixture was prepared by mixing 2.5 μL cDNA (∼25 ng) with 12.5 μL SYBR Green PCR Master Mix (Thermo Fisher Scientific), 0.25 μL each of the forward and reverse primers (Table S1; 0.25 pmol), and 9.5 μL deionized water. The used PCR conditions were: 4 minutes at 94°C, followed by 35 cycles of 30 seconds at 94°C, 30 seconds at 60°C, and 45 seconds at 72°C. qRT-PCR was performed in 96-well microtiter plates using an iQ5 thermal cycler (Bio-Rad). Experiments were carried out in triplicate. At the end of every run, a melting curve analysis was performed. Results were analyzed with the ΔΔCt method,[17] and the enolase gene (*STY3081*) was used to normalize the corresponding cycle threshold (Ct) values.

2.2 | styMdtM construct generation and site-directed mutagenesis

Site-directed mutagenesis using the QuikChange PCR method (Stratagene) was used to generate the pMR4-styMdtM-TEV-His$_8$ construct by introducing a tobacco etch virus (TEV) protease cleavage site before the C-terminal His$_8$ tag in the pMR4-STY4874-His$_8$ construct generated previously.[15] The strategy used is shown in Figure S1[18] and the primer sequences are listed in Table S1. Site-directed mutagenesis was also used to introduce the Asp25Ala, Asp25Glu, Arg111Ala, and Arg111Lys substitutions, using miniprep DNA of pMR4-styMdtM-TEV-His$_8$ as the template (Figure S2) and the primers listed in Table S1. The open reading frame and mutations of all constructs were verified by DNA sequencing.

2.3 | Determination of the minimum inhibitory concentration

The minimum inhibitory concentration (MIC) of various compounds was determined according to the guidelines of the Clinical and Laboratory Standards Institute (http://www.clsi.org/). MIC assays were carried out using the 2-fold agar dilution method[19] and *E. coli* strain KAM42, which is deficient in the AcrB, TolC, and YdhE efflux transporters.[20]

2.4 | Expression and purification of wild-type styMdtM and mutant proteins

E. coli strain C41(DE3)[21] was transformed with expression constructs for wild-type or mutant styMdtM. The transformed cells were grown

at 37°C first on LB agar plates containing 100 μg/mL ampicillin and 0.2% (wt/vol) glucose, and then in LB broth with shaking at 200 rpm to prepare precultures. The precultures (1%, vol/vol) were used to inoculate LB broth containing 100 μg/mL ampicillin and 0.04% (wt/vol) glucose, and the cultures were grown at 37°C with shaking at 200 rpm. When OD_{600} reached 0.6, the temperature was lowered to 30°C and after approximately 1 hour, when OD_{600} reached 0.8 to 1.0, protein expression was induced by adding 0.1 mM isopropyl thiogalactopyranoside (IPTG). After an additional 3-hour incubation at 30°C with shaking at 200 rpm, cells were harvested by centrifugation at 5000g for 10 minutes at 4°C.

For membrane preparation, cells from 10 to 12 L of cell culture were resuspended in 20 mM Tris-HCl, pH 7.5, 0.5 mM ethylenediaminetetraacetic acid (EDTA), 1 mM phenylmetylsulfonyl fluoride (PMSF) and two tablets of protease inhibitor cocktail (Roche) and disrupted by passing them 2 to 3 times through an Avestin French press at 15 kpsi. Cell debris was removed by centrifugation at 12000g for 45 minutes at 4°C. The supernatant was centrifuged at 100 000g for 90 minutes at 4°C to collect the membranes. The membranes were washed with 20 mM Tris-HCl, pH 7.5, and stored at −80°C until use.

For protein purification, membranes (at a protein concentration of 3 mg/mL) were solubilized with 1% (wt/vol) n-dodecyl-β-D-maltopyranoside (DDM) in 20 mM Tris-HCl, pH 7.5, 100 mM NaCl, 2 mM β-mercaptoethanol (β-ME), 5 mM imidazole, and 1 mM PMSF for 1 hour at 25°C with shaking at 125 rpm, and purified by nickel-affinity chromatography as described.[18] The His_8 tag was removed by incubation with TEV protease and dialyzing the protein solution against 20 mM Tris-HCl, pH 7.5, 100 mM NaCl, 0.04% (wt/vol) DDM, 10% (vol/vol) glycerol, and 1 mM dithiothreitol. The protein was concentrated to approximately 10 mg/mL using a 50-kDa cut-off concentrator (Millipore) at 4°C and further purified by gel-filtration chromatography in 20 mM Tris-HCl, pH 7.5, 100 mM NaCl, and 0.04% (wt/vol) DDM, using a Superdex 200 column. The protein concentration was measured using the BCA kit (Pierce).

2.5 | Fourier transform infrared spectroscopy

For Fourier transform infrared (FTIR) measurements, purified protein was dialyzed in a dialysis cassette (3.5 kDa cut-off) against 10 mM potassium phosphate, pH 7.4, 0.04% (wt/vol) DDM for 16 hours at 4°C. The protein was concentrated to 2 to 3 mg/mL by lyophilization, and FTIR spectra were then recorded as described.[22] Briefly, FTIR spectra were recorded with a Bruker FTIR spectrometer in the range of 4000 to 500 cm^{-1} in absorbance mode at 1 nm resolution, 256 scans co-addition and Blackman-Harris-3-term apodization. Buffer-corrected protein spectra were adjusted until a flat baseline was obtained in the region between 2000 and 1770 cm^{-1}. When required, residual vapor absorption was also subtracted. For secondary structure analysis, the second derivative of the amide I region (1700-1600 cm^{-1}) was obtained using the Origin software version 7.0 (Origin Lab Corporation, USA). Before performing second-derivative analyses, spectra were smoothened using two adjacent points. The amide I region was decomposed into individual bands using the Galactic PeakSolve software (version 1.05). Bands used to interpret the spectra were assigned based on previous measurements.[23,24]

2.6 | Circular dichroism spectroscopy

For circular dichroism (CD) measurements, purified protein was dialyzed in a dialysis cassette (3.5 kDa cut-off) against 10 mM potassium phosphate, pH 7.4, 0.04% (wt/vol) DDM for 16 hours at 4°C. CD spectra were recorded as described[25] using an AVIV Model 400 spectropolarimeter equipped with thermoelectric temperature control and calibrated with d10-camphorosulfonic acid, with constant nitrogen flushing. CD spectra (185-250 nm) and thermal unfolding curves were recorded from 0.02 mg/mL protein solutions placed into10-mm quartz cells. The spectra were recorded with a 1-nm bandwidth, 1-nm increments, 15-second response time, and averaging 10 scans. Thermal unfolding data at 222 nm were recorded by heating the sample from 20 to 80°C using 1°C increments, 15-second accumulation time per data point, and a 60-second equilibration time at each temperature.

After subtracting the spectrum of the phosphate buffer from those of the protein solutions, CD spectra were analyzed using the protein concentration-independent method provided by the web-based server (http://perry.freeshell.org/raussens.html),[26] the DichroWeb server (http://dichroweb.cryst.bbk.ac.uk/html/home.shtml),[27,28] the program CONTIN/reference set 3[29] and with a method based on neural networks.[30]

2.7 | Determination of apparent dissociation constants (K_d)

Intrinsic tryptophan fluorescence quenching was used to determine the substrate-binding affinity of detergent-solubilized styMdtM. Fluorescence was measured at 25°C with a Fluoromax-4 fluorometer using excitation and emission wavelengths of 290 and 325 nm, respectively. Freshly purified protein was titrated with different substrates until fluorescence quenching was achieved. The final fluorescence intensity for substrates was corrected by subtracting the quenching buffer. To calculate the apparent "K_d" for substrate binding, data were analyzed by nonlinear regression using the following equation:

$$Fractional\ fluorescence\ quenching\ (\Delta F) = \Delta Fmax \times x / K_d + x,$$

where "$\Delta Fmax$" is the total change in fluorescence and "x" is the substrate concentration.

2.8 | Negative-stain electron microscopy (EM)

2-μL aliquots (10-20 μg/mL) of wild-type or mutant styMdtM were applied to glow-discharged carbon-coated copper-palladium grids and

incubated for 30 seconds. Grids were washed twice with double-distilled deionized water, once with 0.75% (wt/vol) uranyl formate, and then stained for 30 to 40 seconds with 0.75% uranyl formate. Grids were blotted with filter paper and completely dried with vacuum suction. Grids were inspected with a Philips CM10 electron microscope operated at 100 kV and equipped with a Gatan 2 K x 2 K CCD camera (Model 894 US1000). Images were recorded at a defocus of −1.5 μm.

2.9 | Homology model for styMdtM and analysis of helix interactions

The sequence of styMdtM (Uniprot ID: Q8XFG0) was retrieved from UniProt KB[31] and submitted to NCBI-Protein BLAST, which identified *E. coli* MdfA (ecMdfA) as the closest homolog with known structure (PDB ID: 4ZOW).[32] After aligning their sequences in Clustal Omega,[33] Modeler 9v16 (Reference 34) was used to generate a homology model for styMdtM using the structure of ecMdfA as template. The homology model for styMdtM was optimized by energy minimization in AMBER,[35] and the structural and stereochemical properties of the refined model were validated with the programs PROCHECK[36] and ERRAT.[37]

To study helix interactions, the refined homology model was analyzed with DIMPLOT, part of the LigPlot+ software package,[38] using default criteria for hydrogen-bond calculations and nonbonded contact parameters.

3 | RESULTS

3.1 | Clinical isolates of *Salmonella* Typhi constitutively express the *styMdtM* gene

We obtained clinical isolates of *S*. Typhi with different resistance profiles from the repository of the National Institute for Biotechnology and Genetic Engineering (NIBGE), Faisalabad, Pakistan. Their resistance profiles[39] are summarized in Table S2. We used quantitative real-time reverse transcriptase PCR (qRT-PCR) to investigate whether these clinical isolates express the *styMdtM* gene and found that all tested *S*. Typhi isolates did express the *styMdtM* gene (Figure 1).

3.2 | Residues Asp25 and Arg111 are critical for the styMdtM transport function

The structure and mechanism of *Salmonella* sp. MdtM transporters have not yet been studied, but information is available for its close homologs in *E. coli*, ecMdfA and ecMdtM.[40-42] Since previous studies showed that the charged residues Glu26 and Arg112 in ecMdfA and Asp22 and Arg108 in ecMdtM (Figure S2) play critical roles in substrate transport,[41,42] we decided to study the corresponding Asp25 and Arg111 residues in styMdtM. Asp25 is a proton-titratable residue
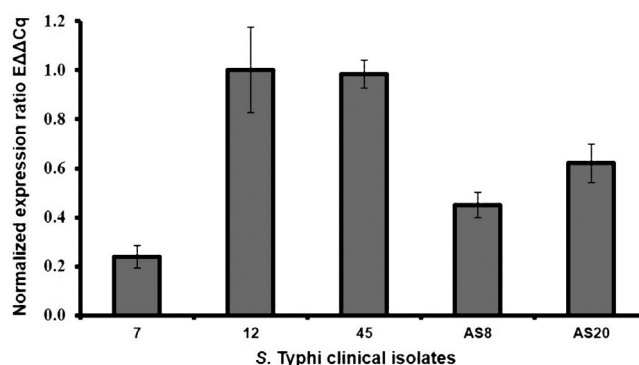

FIGURE 1 qRT-PCR analysis of *styMdtM* gene expression in different *S*. Typhi isolates. The expression of the *styMdtM* gene was normalized to the expression of the enolase housekeeping gene. Error bars represent the SD from three independent experiments. qRT-PCR, quantitative real-time reverse transcriptase PCR

and may thus play a role in the proton-coupled substrate translocation mechanism used by styMdtM,[15] whereas Arg111 is part of characteristic motif B (lxxxRxxqGxgaa) that is highly conserved in MFS proteins.[15]

Substrate profiling showed that the charge-preserving mutation Asp25Glu did not affect the transport function of the mutant protein, but the Asp25Ala mutation abolished transport of all tested substrates (Table S3). This result shows that the transport function does not depend on Asp25 per se, but does require a negatively charged residue at this position, possibly directly contributing to the proton-coupled translocation of antimicrobials. In contrast, for Arg111, both the alanine as well as the charge-preserving Arg111Lys mutation completely abolished the styMdtM transport function (Table S3), indicating that an arginine residue at this position is an absolute requirement.

3.3 | Residue Arg111, but not Asp25, is required for the structural integrity of styMdtM

Substrate profiling showed that the Asp25Ala, Arg111Lys, and Arg111Ala point mutations rendered the transporter inactive. Possible reasons for the inactivation include that the mutations cause the transporter to misfold, interfere with substrate recognition and/or binding, and/or impair substrate translocation. To distinguish between these possibilities, we set out to purify the wild-type and inactive mutant styMdtM transporters, and to analyze their secondary-structure content and substrate-binding capacity. While we could purify the wild-type transporter as well as the Asp25Ala and Arg111Ala mutants in dodecyl maltoside (DDM), despite several attempts, we were not able to purify, and hence further characterize, the Arg111Lys mutant.

The purified wild-type styMdtM protein migrated on SDS-PAGE gels as a major band of ~34 kDa (Figure 2A). While this mass is smaller than the molecular mass calculated from its amino acid sequence
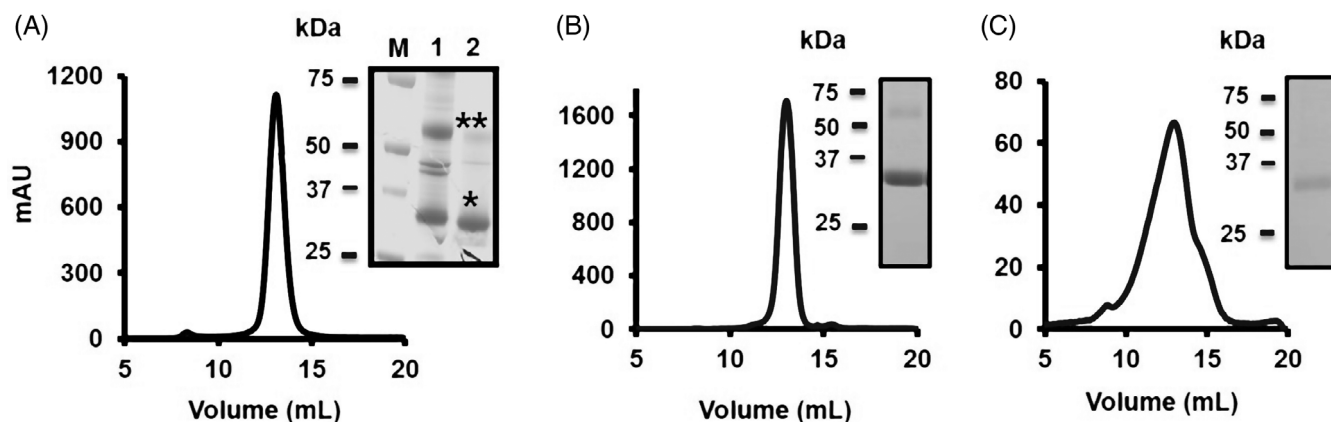
FIGURE 2 Purification of wild-type styMdtM and alanine mutants in DDM. styMdtM constructs with a TEV protease-cleavable C-terminal His$_8$ tag were expressed in *E. coli* at 30°C. Shown are traces from the final size-exclusion chromatography column and Coomassie Brilliant Blue-stained SDS-PAGE gels of the peak fractions (insets). A, Wild-type styMdtM. M: molecular weight markers; lane 1: purified protein before digestion with TEV protease; lane 2: purified protein after digestion with TEV protease. * and ** above the bands indicate monomeric and oligomeric styMdtM species. B, Asp25Ala mutant styMdtM after removal of the His$_8$ tag. C, Arg111Ala mutant styMdtM after removal of the His$_8$ tag. DDM, n-dodecyl-β-D-maltopyranoside; TEV, tobacco etch virus

(46.6 kDa), Western blots with anti-His antibody confirmed the band to contain styMdtM.[15] Furthermore, mass spectrometry analysis identified the additional band seen at ~55 kDa also as styMdtM, suggesting that it represents an oligomer (Figure 2A). The sharp peak eluting from the gel-filtration column indicates that the protein is mono-disperse (Figure 2A), which is consistent with the homogeneous particle population seen in electron micrographs of negatively stained samples (Figure S3).

The functionally inactive mutants were purified in the same way as wild-type styMdtM. The gel-filtration profile and SDS-PAGE gel of purified Asp25Ala mutant were comparable to the wild-type transporter (Figure 2B) and also showed mono-disperse particles in negative-stain EM images (Figure S3). In contrast, yields of the Arg111Ala mutant were low, and the purified protein appeared less stable once extracted from the membrane. While gel filtration showed a broader peak, SDS-PAGE analysis of the peak fraction did show the expected band at ~34 kDa (Figure 2C) and the particles looked mono-disperse in negative-stain electron microscopy images (Figure S3).

To better assess the structural integrity of the mutants, we measured their secondary-structure content.[43] We first analyzed wild-type styMdtM by both FTIR and CD spectroscopy (Figure 3A). For quantitative analysis of the FTIR spectrum, the second derivative was calculated after the buffer contribution was subtracted from the spectrum. The amide I region (1700-1600 cm^{-1}) was then decomposed into individual bands (Figure 3B). Analysis of the amide I region of the wild-type styMdtM spectrum suggested an α-helical content of ~55% (Table S4). Quantitative analysis of the CD spectrum of wild-type styMdtM (Figure 4A), using a number of protein concentration-dependent and -independent methods, predicted that styMdtM has an α-helical content between 53% and 69% (Table S4). Taken together, CD and FTIR spectroscopy confirmed that styMdtM purified in DDM retains a high α-helical content, which is a characteristic of inner membrane proteins from gram-negative bacteria[18] and is

expected for styMdtM considering that the homologous ecMdfA and ecMdtM transporters contain 12 transmembrane α-helices.[40-42] Moreover, in-silico analysis of the secondary structure using the TMHMM server also predicts an α-helical content of 63% for this transporter (Table S4).[44]

After ascertaining the predominantly α-helical nature of styMdtM, we used CD spectroscopy to characterize the mutant proteins. The CD spectrum of the Asp25Ala mutant was very similar to that of wild-type styMdtM, but not that of the Arg111Ala mutant (Figure 4A). Accordingly, the α-helical content of the Asp25Ala mutant was comparable to that of wild-type styMdtM (69% and 67%, respectively), but that of the Arg111Ala mutant was considerably higher (~95%).

To further assess the structural integrity of the styMdtM variants, the proteins were subjected to thermal unfolding while monitoring the CD ellipticity at 222 nm. The unfolding (melting) curve of the Asp25Ala mutant showed similar gradual disruption of the secondary structure as wild-type styMdtM (Figure 4B), indicating that the mutant protein was correctly folded and retained its structural integrity. However, the melting curve for the Arg111Ala mutant looked very different, suggesting that substituting Arg111 with alanine compromised the structural integrity of the protein (Figure 4B). Taken together, these results suggest that the Asp25Ala mutation likely interferes with substrate binding or transport as it does not affect the protein structure, whereas Arg111Ala mutation most likely interferes with the activity of styMdtM by destabilizing its structure.

3.4 | Residue Asp25 is required for substrate translocation

To determine whether the Asp25Ala mutation interferes with substrate binding or substrate translocation, we used an intrinsic
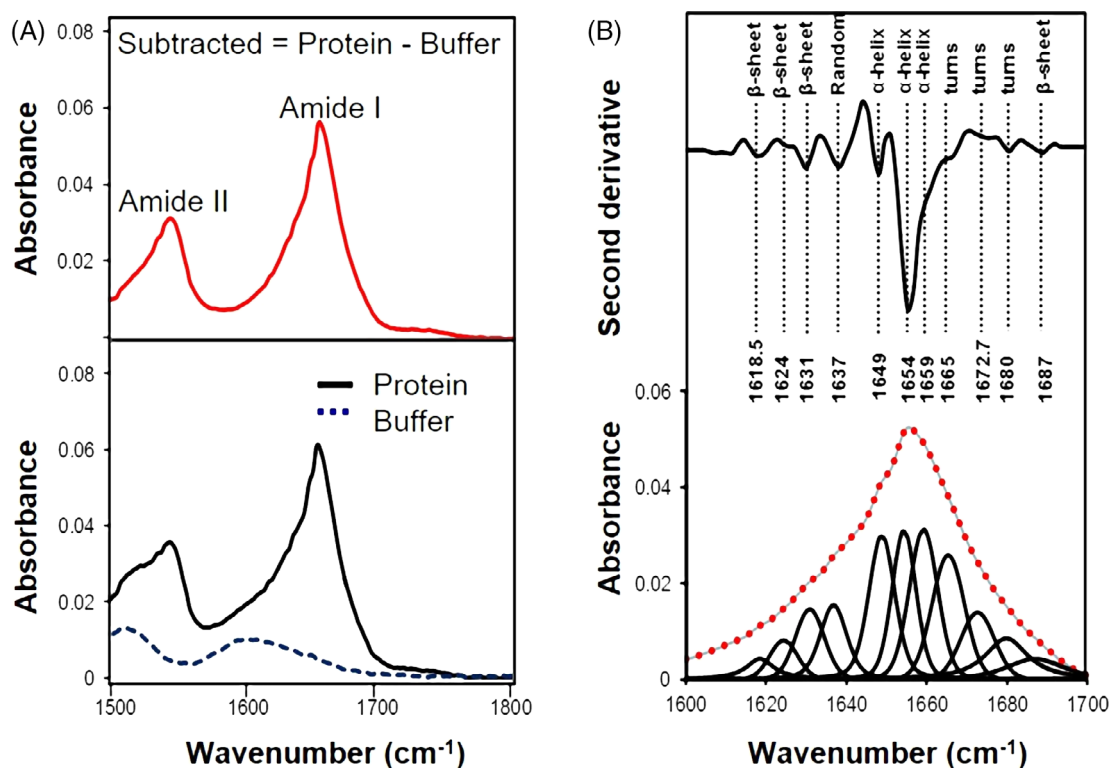
FIGURE 3 FTIR spectrum of purified styMdtM in DDM. A, Lower panel: FTIR spectra of hydrated films of Tris buffer and styMdtM protein solution. Upper panel: Final FTIR spectrum for styMdtM obtained by subtracting the buffer spectrum from that of the protein solution. B, Second derivative of the amide I region in the FTIR spectrum of a hydrated film of styMdtM (top), and bands obtained by deconvolution (bottom). The dotted red line shows the curve that was fitted using the component bands. The peak positions of the spectral components along with their assignments are shown. DDM, n-dodecyl-β-D-maltopyranoside; FTIR, Fourier transform infrared
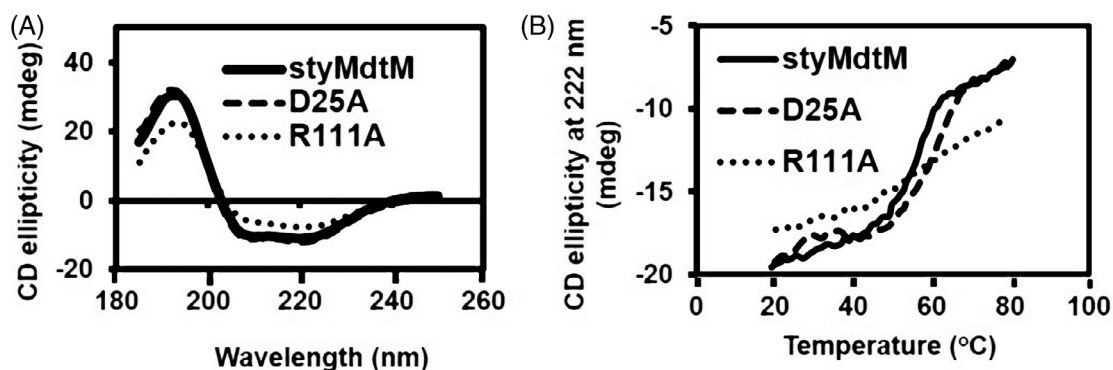

FIGURE 4 CD spectra and melting curves of wild-type and mutant styMdtM in DDM. A, CD spectra of the wild-type and alanine mutant transporters. B, Melting curves for the wild-type and mutant transporters as measured by the CD ellipticity at 222 nm. CD, circular dichroism; DDM, n-dodecyl-β-D-maltopyranoside

fluorescence-based approach to assess the substrate-binding capability of the mutant. The styMdtM protein (NP_458943.1) contains nine tryptophan and seven tyrosine residues. It was thus likely that substrate binding would lead to changes in the intrinsic protein fluorescence. Indeed, the intrinsic fluorescence of DDM-solubilized styMdtM changed in the presence of the known substrates[15] streptomycin, gentamycin, kanamycin, and chloramphenicol. This allowed us to measure substrate-binding curves, from which we

could deduce the apparent dissociation constants (K_d) for the substrates (Figure 5). The results revealed that styMdtM has high-binding affinity for streptomycin and gentamycin, with apparent K_d values of 0.02 ± 0.004 μM (Figure 5A) and 0.05 ± 0.006 μM (Figure 5B), respectively. The binding affinity of styMdtM for kanamycin and chloramphenicol were comparatively lower, with apparent K_d values of 0.24 ± 0.04 μM (Figure 5C) and 0.617 ± 0.021 μM (Figure 5D), respectively.
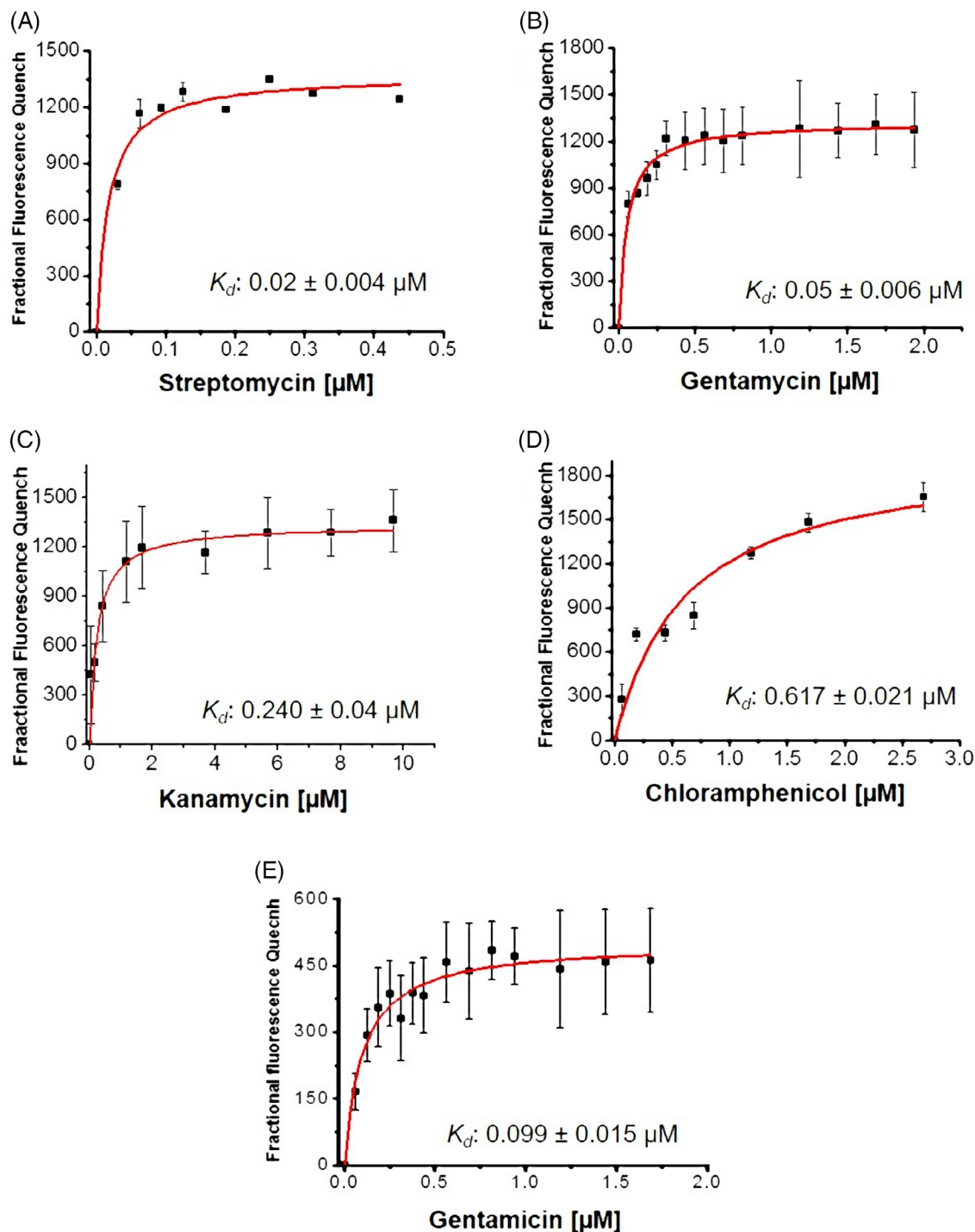
FIGURE 5 Substrate binding to purified styMdtM in DDM. The panels show concentration-dependent substrate binding to styMdtM. A-D, Binding of streptomycin A, gentamycin B, kanamycin C, and chloramphenicol D to wild-type styMdtM. E, Binding of gentamycin to Asp25Ala mutant styMdtM. Data points are shown as mean and SD from three independent measurements. DDM, n-dodecyl-β-D-maltopyranoside

To evaluate the effect of the Asp25Ala mutation on substrate binding, we measured the binding curve of the mutant transporter for gentamicin, one of the substrates with higher binding affinity. The apparent K_d of the Asp25Ala mutant for gentamicin binding was 0.099 ± 0.015 μM (Figure 5E). These results suggest that the Asp25Ala mutant retains the ability to bind gentamicin, although expression of this mutant did not protect cells from the antimicrobial effect of gentamicin (Table S3).

3.5 | Residue Arg111 stabilizes the styMdtM fold by mediating helix-helix interactions

Despite multiple attempts, we were not able to purify the Arg111Lys mutant, and while we were able to purify the Arg111Ala mutant, its structural integrity was compromised. It thus appears that an arginine at position 111 is required for the structural

integrity of styMdtM. To evaluate this notion, we generated a homology model for styMdtM.

A protein database search established that with a sequence identity of 36.96% and a sequence similarity of 59.42% (Figure S4), ecMdfA is the closest homolog of styMdtM with a known structure. In addition to their high-sequence similarity, both of these MDR pumps can transport chloramphenicol. We thus used the crystal structure of ecMdfA with bound chloramphenicol (PDB ID: 4ZOW)[32] as the template to build an energy-minimized homology model for sty-MdtM in the inward-facing conformation (Figure S5A). Comparison of the backbone atoms of the final styMdtM model with the corresponding ones in the ecMdfA crystal structure yielded an RMSD of 0.49 Å (Figure S5B).

The refined styMdtM homology model was evaluated with the ERRAT program,[37] which has proven very accurate in judging the reliability of homology models, yielding an overall quality factor for the model of 100% (Table S5). Analysis of the homology model with PROCHECK showed that 99.7% of the residues fall into the favorable

and allowed regions, while only 0.3% of the residues, namely His404, which is not part of the active site and is not involved in the stabilization of the structure, lies in a disallowed region (Figure S6). The quality evaluation values for the homology model before and after energy minimization are summarized in Table S5.

The homology model of styMdtM in the inward-facing conformation shows the typical MFS fold, which is composed of an N- and a C-terminal domain with each containing 6 transmembrane α-helices (TMs) joined by short loops. The two domains are connected by an interdomain loop of 27 residues that contains a short α-helix (Figure S7). TMs 3, 6, 9, and 12 are peripheral, while the remaining TMs form the substrate-translocation pathway at the interface between the two domains.

The residues mutated in this study lie on TMs, with Asp25 located more toward the cytoplasmic side of TM1 and Arg111 located more toward the periplasmic side of TM4 (Figure 6). The negatively charged side chain of Asp25 extends into the substrate-translocation pore (Figure 6), consistent with the notion that
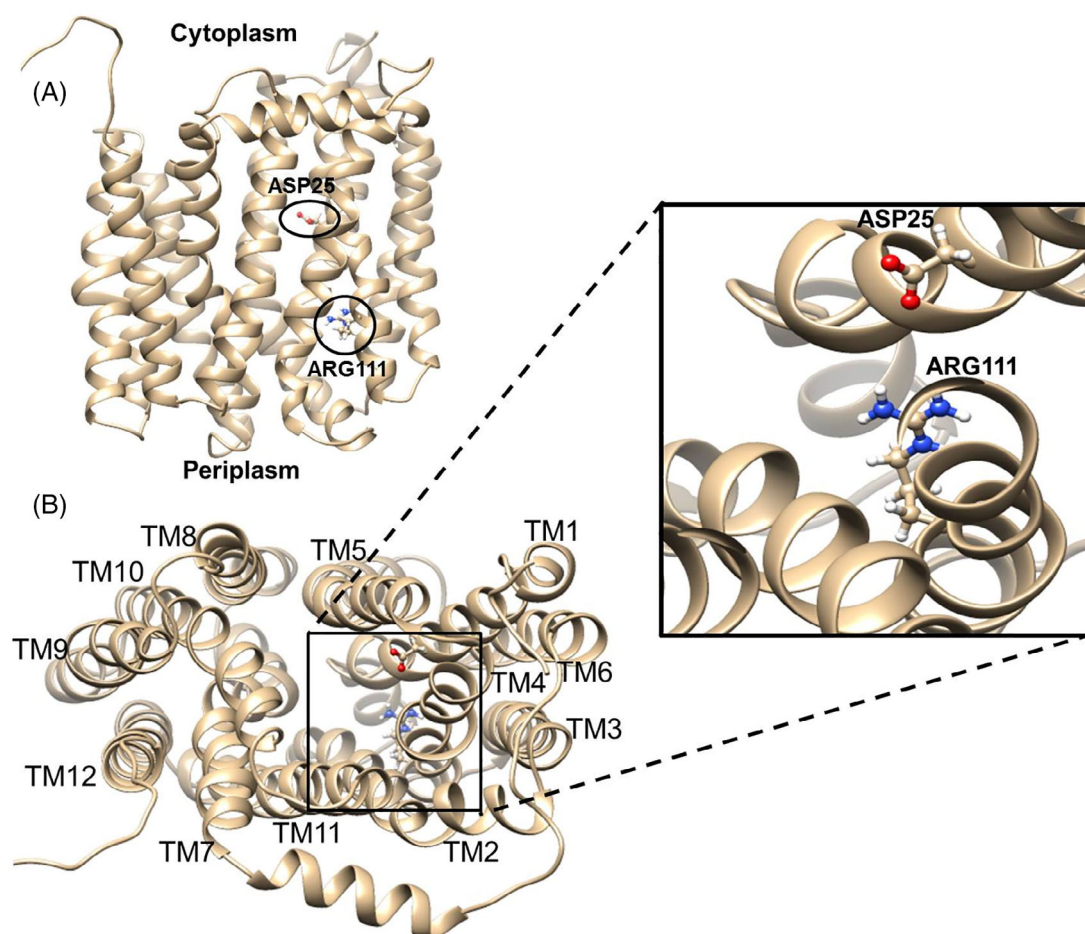

FIGURE 6 Homology model of styMdtM. A, View of the homology model parallel to the membrane. The protein is shown in ribbon representation and residues Asp25 and Arg111 in ball-and-stick representation. B, View of the homology model from the cytoplasmic side. The Asp25 residue extends into the substrate-translocation pathway. Replacing this residue with a neutral residue does not affect the structure or prevent substrate binding, but abolishes substrate translocation. The inset shows that the Arg111 residue is located where helix IV interacts with helix I. Mutating this residue destabilizes the structure of the transporter
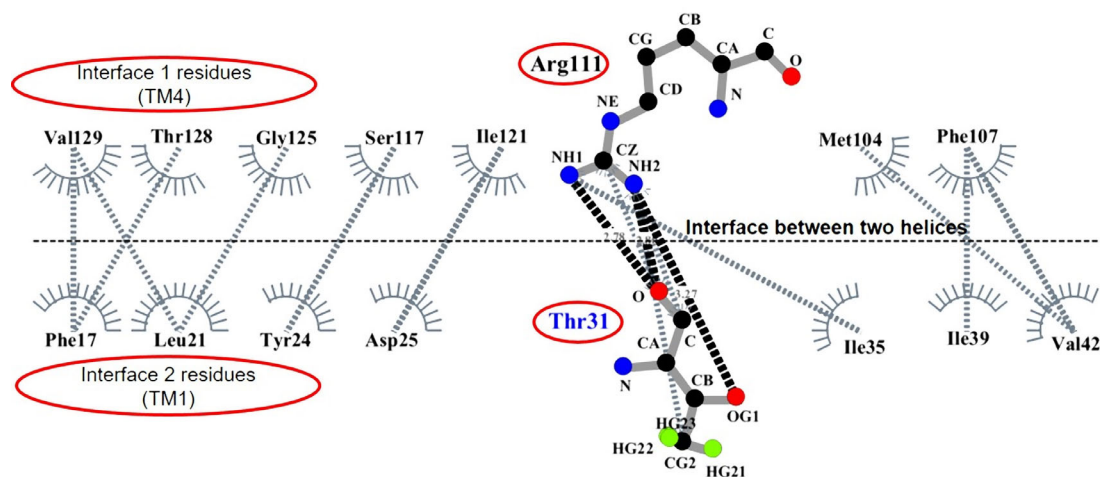
FIGURE 7   Helix-helix interactions predicted by DIMPLOT. A search for helix-helix interactions between TM1 (residues 7-45) and TM4 (residues 104-132) shows that eight residues from each helix are involved in the interaction. TM4 residue Arg111 forms three hydrogen bonds with TM1 residue Thr31. Arg111 also forms hydrophobic interactions with Thr31 and Ile35. In contrast, TM1 residue Asp25 only forms a single hydrophobic interaction with TM4 residue Ile121. Hydrophobic interactions are shown as gray dashed lines, hydrogen bonds as black dashed lines, and the atoms of Arg111 and Thr31 are color-coded (C: black, N: blue, O: red, H: green)

replacing it may directly affect substrate transport. In the case of Arg111, its positively charged side chain extends toward neighboring TM1 (Figure 6), indicating a role in stabilizing the structure of the transmembrane domain.

We used the program DIMPLOT to further analyze the interactions of Arg111 with neighboring residues. Using default parameters, the program identified helix-helix interactions that Arg111-containing TM4 (Met104 to Ala132) forms with TM1 (Phe7 to Asp45) and TM3 (Val50 to Ile78). The interaction of TM4 with TM3 does not involve a substantial contribution from Arg111, which only forms hydrophobic contacts with TM3 residues Ser56 and Tyr60. On the other hand, Arg111 contributes substantially to the interaction with TM1. In addition to forming three hydrophobic contacts with TM1 residues Thr31 and Ile35, it also forms three hydrogen bonds with Thr31 (Figure 7). By contrast, Asp25 in TM1 contributes little to interactions with neighboring TMs, forming only a single hydrophobic contact with TM4 residue Ile121 (Figure 7). These observations are consistent with the positively charged Arg residue playing an important part in stabilizing the structure of styMdtM.

4 | DISCUSSION

The currently recommended therapy to treat *Salmonellosis* is fluoroquinolone (FQ), but increasing numbers of *Salmonella* isolates worldwide show resistance against FQ.[1] While the detection of mutations in quinolone resistance-determining regions, in particular in genes encoding DNA gyrase and topoisomerase IV enzymes, provided a molecular explanation for FQ resistance,[45,46] our understanding of the role of MDR transporters that expel antibiotics and potentiate the effect of mutations in quinolone resistance-determining regions remains comparatively poor.

Bacterial MDR transporters are highly conserved proteins that contribute to intrinsic, acquired, and phenotypic resistance to antimicrobials.[47] styMdtM is a member of the MFS and, when expressed under the control of an exogenous promoter from a high-copy number plasmid, expelled many of the tested substrates, making the bacteria resistant to these antimicrobials.[15] styMdtM is thus an effective MDR transporter. We analyzed the expression of styMdtM in clinical *S.* Typhi isolates as compared to the expression of the enolase gene, which has been found to express at the same level in all bacterial samples tested.[48] While the expression levels varied to some degree, all isolates expressed the transporter at a substantial level. Since the isolates were grown in the absence of antibiotics, these results suggest that most, if not all *S.* Typhi express the *styMdtM* gene constitutively. This is in agreement with previous studies on ecMdfA expression in clinical isolates of *E. coli* that found similar results.[49,50] Multiple sequence alignment shows that the *styMdtM* gene is highly conserved in the *Salmonella* genus. Expression of the transporter in all tested isolates suggests that it functions not only as an MDR transporter when the bacteria are exposed to antibiotics, but that it plays an essential physiological role that is needed for bacterial survival. Such a role has already been proposed for the *E. coli* MdtM homolog, which has been suggested to function as a Na$^+$/H$^+$ and K$^+$/H$^+$ antiporter that helps to maintain the cytoplasmic pH in alkaline environments.[51]

Mutagenesis of Asp25 established that substrate transport only requires a negative charge at this position, yielding a functional mutant when aspartate is substituted by glutamate. Notably, the residue corresponding to styMdtM Asp25 in the *E. coli* homolog MdfA is in fact a glutamate (Figure S2). Nevertheless, Asp25 is highly conserved in *Salmonellae*. The importance of the aspartate at this position has also been established for the *E. coli* MdtM homolog. As with styMdtM, the Asp22Ala mutation in ecMdtM, corresponding to the Asp25Ala mutation in styMdtM, also abolishes substrate transport but

only reduces substrate binding to the mutated transporter.[41] Since the transporters do not require this aspartate for substrate binding, the alanine mutations may lock the transporters in a state in which they can bind substrate but can no longer undergo the conformational changes needed for substrate translocation. Since MdtM is an antiporter and substrate translocation thus requires the counter-movement of a proton across the membrane, it is possible that the negative charge at this position is needed for proton translocation. Removal of the negative charge could thus disrupt either proton binding or the proton counter-translocation.

Our homology model of styMdtM in the inward-facing conformation shows the typical architecture of an MFS transporter. This homology model shows Arg111 in TM4 forming extensive interactions with residues in TM1 that likely stabilize the structure of the transmembrane domain, thus explaining the deleterious effect that mutations of this residue have on the stability of the protein. The intricate interactions that Arg111 forms with Thr31 may also explain the counterintuitive result that the non-conservative Arg111Ala mutation has a less destabilizing effect on the structure than the conservative Arg111Lys mutation, as removing positive charges from the hydrophobic core of the membrane may be less disruptive than replacing the positive charges in a way in which they can no longer be properly compensated by hydrogen-bond formation, thus providing a possible explanation for the strongly destabilizing effect of the Arg111Lys mutation.

It is noteworthy that although the *Salmonellae* efflux pumps EmrAB, MdfA, and MdtK have 90% sequence identity with their *E. coli* homologs, the drug specificities of the *Salmonella* transporters differ from those of the corresponding *E. coli* transporters.[52] The reasons for these differences in substrate specificity are yet to be determined, arguing for the necessity to fully characterize the specific MDR transporters expressed in *Salmonellae*. This study reports our contribution toward a comprehensive characterization of an MFS transporter expressed in typhoidal *Salmonella*. Since the styMdtM transporter is conserved in all *Salmonella enterica* subspecies, including *S.* Typhimurium, *S.* Paratyphi, *S.* Enteritidis, and *S.* Newport, the results obtained in this study for *S.* Typhi should be applicable to the other *Salmonella enterica* subspecies.

5 | CONCLUSION

In this study, we show that all tested clinical isolates of *S.* Typhi constitutively express the MDR transporter MdtM, suggesting that, in addition to acting as an acquired resistance determinant, it also has an essential function for bacterial survival. Our mutagenesis experiments together with structural and functional analyses of the mutants suggest that Asp25, or more precisely the negative charge at position 25, is directly involved in substrate translocation, whereas Arg111 is essential in stabilizing the structure of the transporter. Our study thus provides further insights into an MDR transporter from *S.* Typhi, a pathogen that remains a threat to public health in developing

countries in Southeast Asia and Africa, but, due to international travel, also occasionally causes typhoidal cases in Europe and America.

CONFLICT OF INTERESTS

The authors declare that they have no conflict of interest.

PEER REVIEW

The peer review history for this article is available at https://publons.com/publon/10.1002/prot.26141.

DATA AVAILABILITY STATEMENT

The data that supports the findings of this study are available in the supplementary material of this article.

ORCID

Aqsa Shaheen 🄳 https://orcid.org/0000-0002-7887-677X
Fouzia Ismat 🄳 https://orcid.org/0000-0001-6975-8782
Mazhar Iqbal 🄳 https://orcid.org/0000-0002-8675-1125
Abdul Haque 🄳 https://orcid.org/0000-0003-3743-4243
Zaheer Ul-Haq 🄳 https://orcid.org/0000-0002-8530-8711
Osman Mirza 🄳 https://orcid.org/0000-0001-9435-0690
Rita De Zorzi 🄳 https://orcid.org/0000-0001-7001-7498
Thomas Walz 🄳 https://orcid.org/0000-0003-2606-2835
Moazur Rahman 🄳 https://orcid.org/0000-0003-2892-1250

REFERENCES

1. Saeed N, Usman M, Khan EA. An overview of extensively drug-resistant *Salmonella* Typhi from a tertiary care hospital in Pakistan. *Cureus*. 2019;11:e5663.
2. Browne AJ, Kashef Hamadani BH, Kumaran EAP, et al. Drug-resistant enteric fever worldwide, 1990 to 2018: a systematic review and meta-analysis. *BMC Med*. 2020;18:1.
3. Braoudaki M, Hilton AC. Mechanisms of resistance in *Salmonella enterica* adapted to erythromycin, benzalkonium chloride and triclosan. *Int J Antimicrob Agents*. 2005;25:31-37.
4. Sun J, Deng Z, Yan A. Bacterial multidrug efflux pumps: mechanisms, physiology and pharmacological exploitations. *Biochem Biophys Res Commun*. 2014;453:254-267.
5. Davies J, Davies D. Origins and evolution of antibiotic resistance. *Microbiol Mol Biol Rev*. 2010;74:417-433.
6. Cherkasov A, Hilpert K, Jenssen H, et al. Use of artificial intelligence in the design of small peptide antibiotics effective against a broad spectrum of highly antibiotic-resistant superbugs. *ACS Chem Biol*. 2008;4:65-74.

7. Blair JM, Webber MA, Baylay AJ, Ogbolu DO, Piddock LJ. Molecular mechanisms of antibiotic resistance. *Nat Rev Microbiol*. 2015;13: 42-51.

8. Quinn T, O'Mahony R, Baird AW, Drudy D, Whyte P, Fanning S. Multi-drug resistance in *Salmonella enterica*: efflux mechanisms and their relationships with the development of chromosomal resistance gene clusters. *Curr Drug Targets*. 2006;7:849-860.

9. Li XZ, Nikaido H. Efflux-mediated drug resistance in bacteria. *Drugs*. 2004;64:159-204.

10. Chen S, Cui S, McDermott PF, et al. Contribution of target gene mutations and efflux to decreased susceptibility of *Salmonella enterica* serovar typhimurium to fluoroquinolones and other antimicrobials. *Antimicrob Agents Chemother*. 2007;51:535-542.

11. Ferrari RG, Galiana A, Cremades R, et al. Expression of the *marA, soxS, acrB* and *ramA* genes related to the AcrAB/TolC efflux pump in *Salmonella enterica* strains with and without quinolone resistance-determining regions *gyrA* gene mutations. *Braz J Infect Dis*. 2013;17: 125-130.

12. Baucheron S, Le Hello S, Doublet B, Giraud E, Weill FX, Cloeckaert A. *ramR* mutations affecting fluoroquinolone susceptibility in epidemic multidrug-resistant *Salmonella enterica* serovar Kentucky ST198. *Front Microbiol*. 2013;4:213.

13. Chu C, Su L-H, Chu C-H, Baucheron S, Cloeckaert A, Chiu C-H. Resistance to fluoroquinolones linked to *gyrA* and *parC* mutations and overexpression of acrAB efflux pump in *Salmonella enterica* serotype Choleraesuis. *Microb Drug Resist*. 2005;11:248-253.

14. Nikaido H. Multidrug resistance in bacteria. *Annu Rev Biochem*. 2009; 78:119-146.

15. Shaheen A, Ismat F, Iqbal M, et al. Characterization of putative multidrug resistance transporters of the major facilitator-superfamily expressed in *Salmonella* Typhi. *J Infect Chemother*. 2015;21:357-362.

16. Tariq A, Sana M, Shaheen A, et al. Restraining the multidrug efflux transporter STY4874 of *Salmonella* Typhi by reserpine and plant extracts. *Lett Appl Microbiol*. 2019;69:161-167.

17. Livak KJ, Schmittgen TD. Analysis of relative gene expression data using real-time quantitative PCR and the $2^{-\Delta\Delta CT}$ method. *Methods*. 2001;25:402-408.

18. Rahman M, Ismat F, McPherson MJ, Baldwin SA. Topology-informed strategies for the overexpression and purification of membrane proteins. *Mol Membr Biol*. 2007;24:407-418.

19. Wiegand I, Hilpert K, Hancock RE. Agar and broth dilution methods to determine the minimal inhibitory concentration (MIC) of antimicrobial substances. *Nat Protoc*. 2008;3:163-175.

20. Matsuo T, Chen J, Minato Y, et al. SmdAB, a heterodimeric ABC-type multidrug efflux pump, in *Serratia marcescens*. *J Bacteriol*. 2008;190: 648-654.

21. Miroux B, Walker JE. Over-production of proteins in *Escherichia coli*: mutant hosts that allow synthesis of some membrane proteins and globular proteins at high levels. *J Mol Biol*. 1996;260:289-298.

22. Anwar MI, Iqbal M, Yousef MS, Rahman M. Over-expression and characterization of NS3 and NS5A of hepatitis C virus genotype 3a. *Microb Cell Fact*. 2013;12:111.

23. Goormaghtigh E, Cabiaux V, Ruysschaert JM. Determination of soluble and membrane protein structure by Fourier transform infrared spectroscopy. *Subcell Biochem*. 1994;23:329-362.

24. Susi H, Byler DM. Resolution-enhanced Fourier transform infrared spectroscopy of enzymes. *Methods Enzymol*. 1986;130:290-311.

25. Gursky O, Ranjana M, Gantz DL. Complex of human apolipoprotein C-1 with phospholipid: thermodynamic or kinetic stability? *Biochemistry*. 2002;41:7373-7384.

26. Raussens V, Ruysschaert J-M, Goormaghtigh E. Protein concentration is not an absolute prerequisite for the determination of secondary structure from circular dichroism spectra: a new scaling method. *Anal Biochem*. 2003;319:114-121.

27. Whitmore L, Wallace BA. DICHROWEB, an online server for protein secondary structure analyses from circular dichroism spectroscopic data. *Nucleic Acids Res*. 2004;32:W668-W673.

28. Whitmore L, Wallace BA. Protein secondary structure analyses from circular dichroism spectroscopy: methods and reference databases. *Biopolymers*. 2008;89:392-400.

29. Provencher SW, Glockner J. Estimation of globular protein secondary structure from circular dichroism. *Biochemistry*. 1981;20:33-37.

30. Bohm G, Muhr R, Jaenicke R. Quantitative analysis of protein far UV circular dichroism spectra by neural networks. *Protein Eng*. 1992;5: 191-195.

31. UniProt C. UniProt: a hub for protein information. *Nucleic Acids Res*. 2015;43:D204-D212.

32. Heng J, Zhao Y, Liu M, et al. Substrate-bound structure of the *E. coli* multidrug resistance transporter MdfA. *Cell Res*. 2015;25:1060-1073.

33. Sievers F, Wilm A, Dineen D, et al. Fast, scalable generation of high-quality protein multiple sequence alignments using Clustal omega. *Mol Syst Biol*. 2011;7:539.

34. Webb B, Sali A. Comparative protein structure modeling using modeller. *Curr Protoc Bioinform*. 2014;47(5) 6:1-32.

35. Case D, Betz R, Botello-Smith W, et al. *AMBER 2016*. San Francisco: University of California; 2016.

36. Laskowski RA, MacArthur MW, Moss DS, Thornton JM. PROCHECK: a program to check the stereochemical quality of protein structures. *J Appl Cryst*. 1993;26:283-291.

37. Colovos C, Yeates TO. Verification of protein structures: patterns of nonbonded atomic interactions. *Protein Sci*. 1993;2:1511-1519.

38. Laskowski RA, Swindells MB. LigPlot+: multiple ligand-protein interaction diagrams for drug discovery. *J Chem Inf Model*. 2011;51:2778-2786.

39. Afzal A, Sarwar Y, Ali A, et al. Molecular evaluation of drug resistance in clinical isolates of *Salmonella enterica* serovar Typhi from Pakistan. *J Infect Dev Ctries*. 2013;7:929-940.

40. Edgar R, Bibi E. A single membrane-embedded negative charge is critical for recognizing positively charged drugs by the *Escherichia coli* multidrug resistance protein MdfA. *EMBO J*. 1999;18: 822-832.

41. Holdsworth SR, Law CJ. Functional and biochemical characterisation of the *Escherichia coli* major facilitator superfamily multidrug transporter MdtM. *Biochimie*. 2012;94:1334-1346.

42. Sigal N, Lewinson O, Wolf SG, Bibi E. *Escherichia coli* multidrug transporter MdfA is a monomer. *Biochemistry*. 2007;46:5200-5208.

43. Wallace BA, Lees JG, Orry AJ, Lobley A, Janes RW. Analyses of circular dichroism spectra of membrane proteins. *Protein Sci*. 2003;12: 875-884.

44. Krogh A, Larsson B, von Heijne G, Sonnhammer EL. Predicting transmembrane protein topology with a hidden Markov model: application to complete genomes. *J Mol Biol*. 2001;305:567-580.

45. Suleyman G, Tibbetts R, Perri MB, et al. Nosocomial outbreak of a novel extended-spectrum beta-lactamase *Salmonella enterica* serotype Isangi among surgical patients. *Infect Control Hosp Epidemiol*. 2016;37:954-961.

46. Rushdy AA, Mabrouk MI, Abu-Sef FA, Kheiralla ZH, Mohamed Abdel-All S, Saleh NM. Contribution of different mechanisms to the resistance to fluoroquinolones in clinical isolates of *Salmonella enterica*. *Braz J Infect Dis*. 2013;17:431-437.

47. Blanco P, Hernando-Amado S, Reales-Calderon JA, et al. Bacterial multidrug efflux pumps: much more than antibiotic resistance determinants. *Microorganisms*. 2016;4:14.

48. Sheikh A, Charles RC, Sharmeen N, et al. *In vivo* expression of *Salmonella enterica* serotype Typhi genes in the blood of patients with typhoid fever in Bangladesh. *PLoS Negl Trop Dis*. 2011;5: e1419.

49. Swick MC, Morgan-Linnell SK, Carlson KM, Zechiedrich L. Expression of multidrug efflux pump genes *acrAB-tolC*, *mdfA*, and *norE* in

Escherichia coli clinical isolates as a function of fluoroquinolone and multidrug resistance. *Antimicrob Agents Chemother.* 2011;55: 921-924.

50. Sarkar S, Bhattacharyya A, Mandal S. YnfA, a SMR family efflux pump is abundant in *Escherichia coli* isolates from urinary infection. *Ind J Med Micro.* 2015;33:139-142.

51. Holdsworth SR, Law CJ. Multidrug resistance protein MdtM adds to the repertoire of antiporters involved in alkaline pH homeostasis in *Escherichia coli*. *BMC Microbiol.* 2013;13:113.

52. Nishino K, Latifi T, Groisman EA. Virulence and drug resistance roles of multidrug efflux systems of *Salmonella enterica* serovar typhimurium. *Mol Microbiol.* 2006;59:126-141.

SUPPORTING INFORMATION

Additional supporting information may be found online in the Supporting Information section at the end of this article.